

Ocean access to a cavity beneath Totten Glacier in East Antarctica

Greenbaum, J.S.* [1], D.D. Blankenship [1], D.A. Young [1], T.G. Richter [1], J.L. Roberts [2, 3], A.R.A. Aitken [4], B. Legresy [2, 5, 6], D.M. Schroeder [7], R.C. Warner [2, 3], T.D. van Ommen [2,3], and M.J. Siegert [8]

[1] Institute for Geophysics, University of Texas at Austin, Austin, Texas, USA

[2] Antarctic Climate & Ecosystems Cooperative Research Centre, University of Tasmania, Private Bag 80, Hobart, Tasmania 7001, Australia

[3] Australian Antarctic Division, Channel Highway, Kingston, Tasmania 7050, Australia

[4] School of Earth and Environment, University of Western Australia, Perth, Western Australia, Australia

[5] CSIRO Oceans and Atmosphere Flagship, Castray Esplanade, Hobart, Tasmania, 7000, Australia

[6] CNRS-LEGOS, 14 Av. E. Belin, 31400, Toulouse, France

[7] Jet Propulsion Laboratory, California Institute of Technology

[8] Grantham Institute and Department of Earth Sciences and Engineering, Imperial College London, London, SW7 2AZ, UK

* Corresponding Author: Jamin S. Greenbaum, jamin@utexas.edu, 512-471-0385

1. Introduction:

The objective of this study is to better understand the potential heat delivery from the open ocean to the Totten Glacier Ice Shelf (TGIS) cavity by inferring the bathymetry of the ice shelf cavity and inner continental shelf with new aerogeophysical data. We apply different data types and analysis techniques to constrain the bathymetry beneath and seaward of the Totten Glacier Ice Shelf (TGIS) and to identify a previously-unknown connection to the TGIS cavity. We apply simple hydrostatic calculations to show that ice over a subglacial trough is floating and radar echo amplitude and specularly analyses to show that it has a bright and smooth basal interface. We use commercially available software and publically available data distributed by the National Snow and Ice Data Center.

2. Bathymetry

2.1. Introduction

The sub-ice shelf and near coastal bathymetry is inverted from airborne gravity data. All gravity inversions are complicated by variations in geology and assumptions must be made about rock densities beneath the ice and seawater if there is no a priori geological information for the area in order to invert for a model of the earth^{1,2}. This is a critical issue for continental passive margins such as the present study area that typically have complex geology due to their role in the breakup of continents and as the sink for low density sediments originating on land. The Sabrina Coast is additionally complicated from orogeny that occurred in the area when it was contiguous with the South Australian Craton in the Mesoproterozoic in an area known as the Albany Fraser Province³. A fault that has been proposed to run beneath the Totten Glacier is thought to be equivalent to the Rodona Fault that has been mapped in modern Western Australia⁴. Subsequent rifting between Australia and Antarctica during the late Jurassic to early Cretaceous further complicates the geology of the area. Given these considerations we apply a forward model reflecting recent findings^{4,5} and a conservative, repeatable inversion approach while using depth to basement estimates⁶, maps of ice rises, and videos of compiled satellite images of grounded icebergs to judge the resulting bathymetry. Depth to magnetic basement solutions were computed using 2-D Werner deconvolution⁶ restricting the result to highlight shallow sources (between 500 m and 10 km from the source) because our interest was in comparing shallow basement solutions to areas where the gravity inversion produced shallow topography.

3.2 Gravity Data

Most gravity lines were flown between 500 and 1000 m above the sea or ice surface at an average speed of 90 m/s. Gravity data were averaged with a 100 second filter, resulting in an along track resolution of ~4.5 km. 5 km line spacing was achieved over a 60 km by 80 km area centered over the calving front of the Totten Glacier. The gravity survey is composed of data collected over five years at multiple flight elevations that used a two-axis stabilized gravimeter (Bell Aerospace BGM-3) and a three-axis stabilized gravimeter (CMG GT-1A) in the last year. The calving front survey flown with the GT-1A was acquired in a single season flying at the minimum practical flight elevation and speed to produce the highest possible resolution with the BT-67 platform. The GT-1A segment was extended seaward of TGIS to blend with existing satellite altimetry-derived bathymetry compilations in areas relatively free of fast ice and icebergs. For the purposes of inverting the entire cavity for this study, all gravity data were upward continued to 2,400 m, the elevation of the highest line included in the survey and careful inter-season leveling was applied.

3.3 Gravity modeling and inversion approach

Five broad activities produced the final, inverted bathymetry used in this analysis:

- A. Construct a database of known depths in the survey area:** This database consists of ice upstream of established grounding lines^{7,8}, published ice rises⁷, and spots where we located grounded icebergs (see the videos of grounded icebergs). No ship tracks are close enough to use in the analysis. This database is important because it provides known depths to which the gravity inversions are later judged and is how we judge the uncertainty of the result (see the uncertainty discussion, below).
- B. Build a series of 2D gravity models to infer the bulk density structure of the study area:** Seven 2D models sampling the survey area were constructed that identified bulk density transitions on the grid east (Law Dome) side of the region and in the cavity. 2D modeling and inversions were computed using the commercial GMSYS software package that implements Talwani's method⁹ for profile modeling. The profile models identified 14 large contrasts that were mapped with their respective density values (Supplemental Figure 1). The most coherent feature we identified during this exercise was a broad 300 kg/m³ contrast generally aligned with the grid east TGIS coastline. While a full geological interpretation of the area is beyond the scope of this report it is possible that this transition is related to the Totten-Rodona Fault that recent work suggests runs along the Totten Glacier⁴. Several other contrasts were identified that were difficult to interpret on their own so their positions were overlain on gridded magnetics and gravity data for a joint interpretation (see below). For our analysis all density transitions were restricted to the top 10km in each model.
- C. Inform the forward model with magnetics analysis and interpretation:** Processed magnetics data were available from recent, related work in East Antarctica⁴. We used these data to jointly interpret the bulk density transitions identified with 2D models with gravity and magnetic anomalies and corresponding shallow depth to basement solutions (Supplemental Figure 1). This interpretation resulted in a simple lateral density model consisting of a fault running along the cavity, two high density areas, and a low density region in Law Dome.
- D. Build a 3D model with density distributions consistent with 2D models and magnetics:** A 3D model was constructed using the same vertical density distribution described above and shown in Figure 2, Panel A. The horizontal density distribution of the top 10km was applied using the model described above by applying the density grid shown in Figure 1 (Panel B) to an-priori seafloor layer initially defined to be constant at -600 mbsl. An initial depth of -600m was chosen because it is close to the average water depth in this area of the continental shelf along the Sabrina Coast¹⁰.
- E. Perform 3D inversion:** 3D models and inversions were computed using the commercial GMSYS-3D software package that implements Parker's method¹¹. The free parameter was the seawater/seafloor horizon initially set to be a constant layer at -600m. The inversion computes a series of topographies until the misfit between the observed and synthetic gravity computed from each shape is minimized (convergence limit = 0.1 (mGal), Lower High-Cut Limit = 0.5, Upper High-Cut Limit = 0.7, regional offset = 0.0). The inversion was run over the entire cavity

including areas with grounded ice. The result was filtered using a single pass of a 9 point Hanning convolution filter to eliminate artifacts.

F. Compute misfit between inverted & measured grounded ice, adjust model, repeat inversion:

The density values and boundaries reflected in Figure 1 (Panel E) were selected after several inversions, each judged by the misfit between the inverted and measured grounded ice bottom elevation from available radar ice thickness measurements.

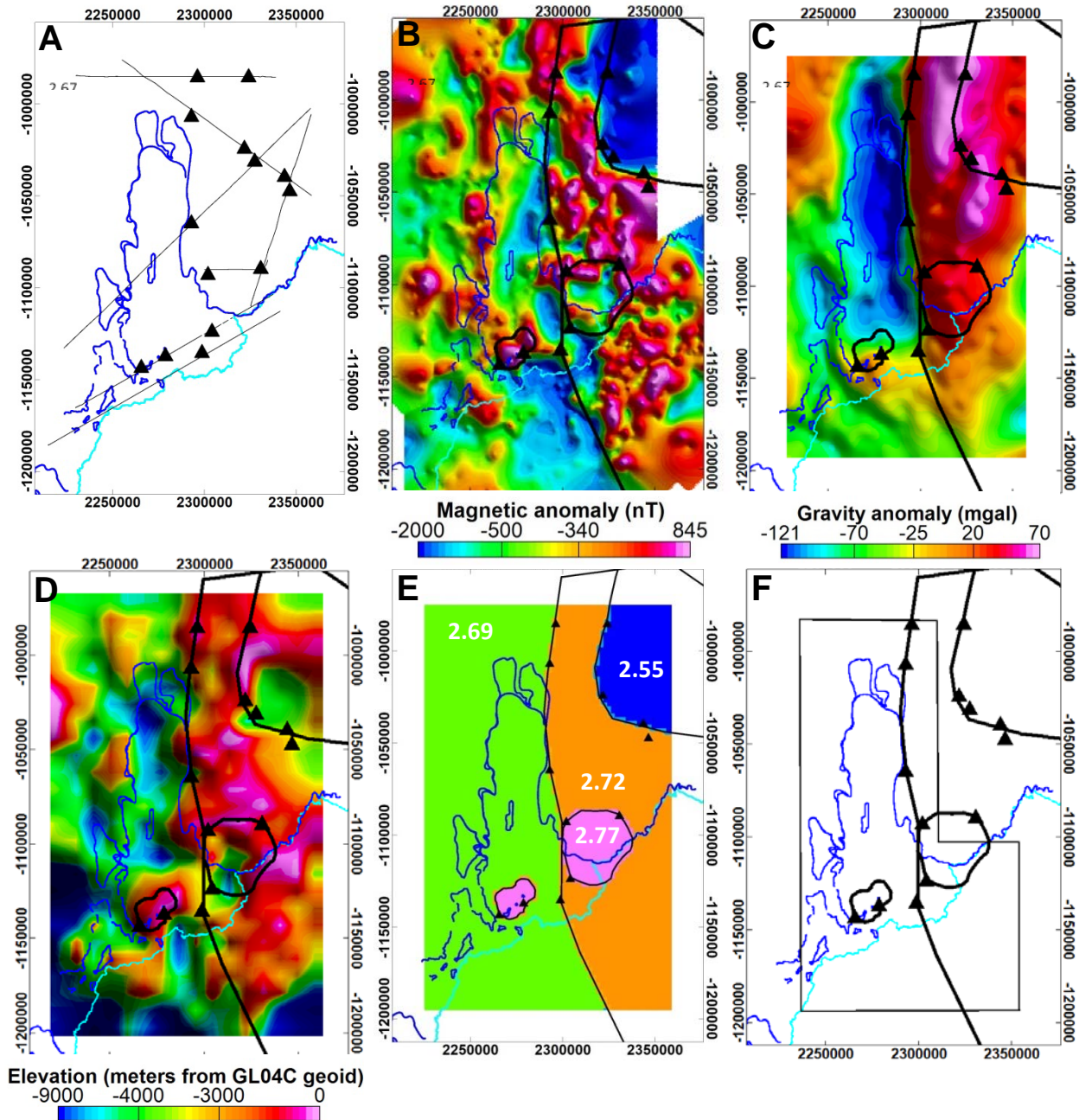


Figure 1 | Horizontal density distribution derivation. Panel A, The survey area with flight lines indicating where 2D gravity inversions were used to infer the location and magnitude of bulk density contrasts. Panels B-D, Gridded Total Magnetic Intensity (TMI) data (nT), Free Air Gravity (mGal), and Depth to Magnetic Basement data used to guide the interpretation of the bulk density contrasts shown in Panel A. Panel E, The horizontal density boundaries (black polygon) and selected bulk density values used in the final inversion. Panel F, Density contrast boundaries plotted with the boundary (black rectangular polygon) used to determine the uncertainties discussed below. The area used for comparison points was chosen to be where the density of gravity lines was high and close to the cavity. The blue and cyan lines in all images represent the grounding line⁷ and ice shelf extent⁸.

3.4 3D Forward Model

The a priori model was composed of six layers. Five layers were fixed and a seafloor/ice bottom layer was left free to move in the inversion. We did not pin the ice bottom layer upstream of the grounding line so that we could use the misfit between the inverted topography where the ice is grounded and radar ice thickness measurements to judge the quality of the geological model and assign an uncertainty to the result (see discussion of uncertainty, below).

The top layer of the model was defined to be the ice surface compiled from airborne laser altimetry measurements with a density set to meteoric ice ($\rho = 0.917 \text{ g/cc}$). The second layer was constructed with radar sounding data and may overlie rock or water since we do not pin the solution to the grounding line. We set the density contrast of the ice bottom layer to seawater ($\rho = 1.03 \text{ g/cc}$); areas that result in no gap between the layers are grounded and those with a gap are floating. The layer below the ice bottom is set to be the inversion layer that is assumed to overlie rock with densities as defined by the polygon in Figure 1 (Panel E). The layer is initially set to be flat at a depth of 600 meters below the GL04C geoid, chosen to approximately match the average seafloor depth of the Sabrina Coast¹⁰. Three flat layers were included to increase the bulk density of the model (this only affects the DC offset): 2.75 g/cc from 10 to 20 km, 2.9 g/cc from 20 to 30km, and 3.3 g/cc below 30km. The depth of the bottom layer was chosen based on deep seismic work that identified the moho at $30 \pm 2 \text{ km}^5$ approximately 200 km from Totten Glacier at Casey Station. The bottom of the model was set to -40km .

The horizontal and vertical density model configurations are illustrated in Figures 1 and 2. The choice of particular density values is somewhat arbitrary because the inversion automatically removes a DC offset that would result from incorrect bulk densities. Our objective is to build a forward model that is close enough to reality that the inversion converges on a better solution than it would otherwise (judged using our database of grounded ice). We have no knowledge of realistic densities in the area so our emphasis was on locating density boundaries which do have a measurable impact on the result.

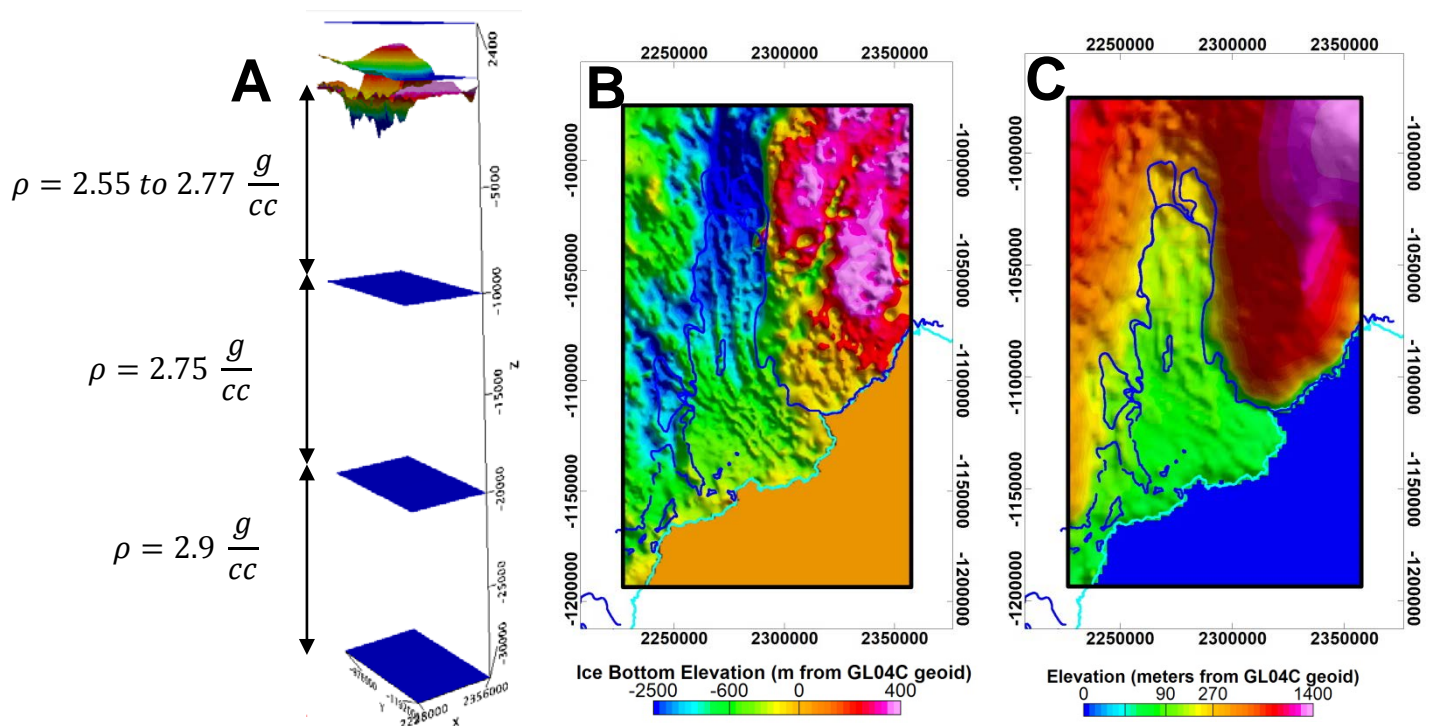


Figure 2 | Vertical density model and ice layers. Panel A, Vertical density distribution; **Panel B**, radar sounding-derived ice bottom elevation input grid, **Panel C**, airborne laser altimetry-derived input grid. The seafloor inversion layer is initially defined as flat at a depth of 600 m below the GL04C geoid to match the average continental shelf depth in the area¹⁰.

3.5 3D Inversion Uncertainty Estimation

Source of uncertainty in gravity inversions include lack of geology knowledge of the study area, instrumentation noise, interpolation errors, and the smoothing effect of the moving platform. We are interested in the absolute error of the inversion from the true shape of the rock interface. Although we do not know the shape of the upper rock layer where the ice is floating, radar sounding provides this geometry where the ice is grounded. Due to the airborne coverage of the survey area we have high resolution rock layer information relative to the resolution of the gravity inversion so comparing the inversion with the geometry of the grounded ice provides a measure of the uncertainty beneath the floating ice if we accept the assumption that the roughness and density of the rock layer is similar between the floating and grounded areas.

Following the literature² we quote the Root Mean Square Error (RMSE) and mean offset between the ice bottom measured by radar sounding and sampled from the bathymetry model inverted from gravity data as the uncertainty in the 3D inversion. Figure 3 shows the radar data used to compute the statistics. The black comparison points cover a large area around the TGIS, the purple and red points ('B' and 'C', respectively) focus on the landward and seaward halves of the TGIS. We use the largest of the three (190 m) to plot the error bars in the main text.

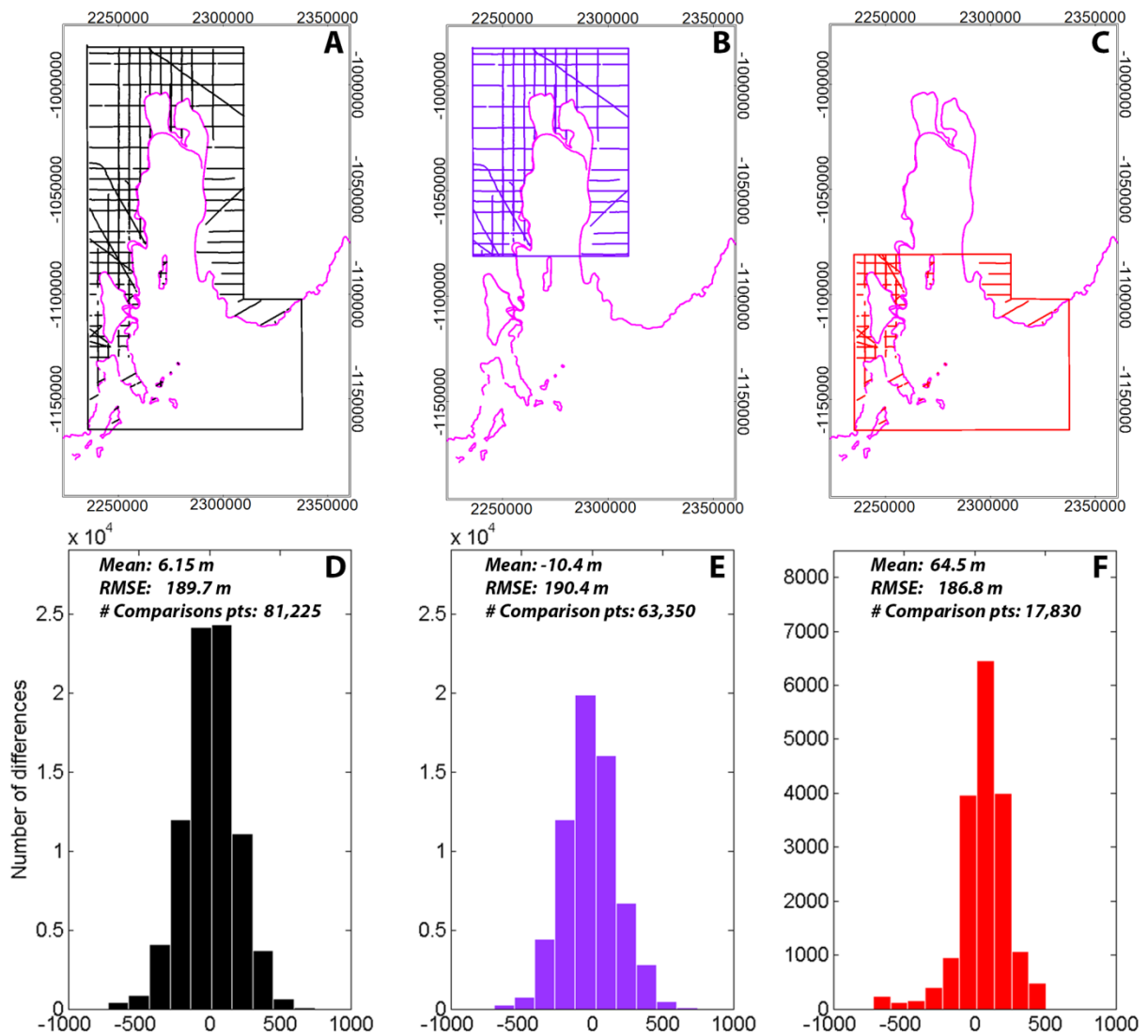


Figure 3 | Uncertainty estimation using known ice bottom elevations. Top row: Points used to compare the inversion result to grounded ice areas for **Panel A**, the entire cavity, **Panel B**, the landward half of the cavity including the deepest grounding line area, and **Panel C**, the seaward half of the cavity. **Panels D-F:** Histograms for the three comparison areas with the Mean and Root Mean Square Error between inverted and measured ice bottom elevations labeled for each.

4. Trough Gravity Data

Two flight profiles (Profiles D-D' and C-C' Figures 4-6, below) recovered gravity data over the newly-discovered trough (trough "X" in Figure 4 below). The two profiles produced similar features for the trough and immediately surrounding area, despite both having been acquired in with a 2-axis gravimeter under sub-optimal flight conditions. Profile D-D' was flown East-to-West and crossed the trough close to the beginning of the line so data quality is lower than for the remainder of the line. Profile C-C' was longer, however, most of the line was flown with a constant (but gentle) altitude change to keep the ice surface within range of the laser altimeters which caused additional accelerations and a higher noise floor. Nevertheless, we have confidence in generally interpreting the result because the two lines independently produce similar features over the trough as shown in Figures 5 and 6.

Both profiles C-C' and D-D' show gravity lows where we interpret a trough based on radar data (between the vertical red lines in both Figures 5 and 6). The signal is small in each case (4 mgal and 2 mgal) but the similarity in size, shape, and location between lines is very unlikely to happen by chance. Although the signal is low, it is short wavelength, indicating that it is due to a near-surface anomaly which supports our interpretation that it is from a trough with steep sidewalls.

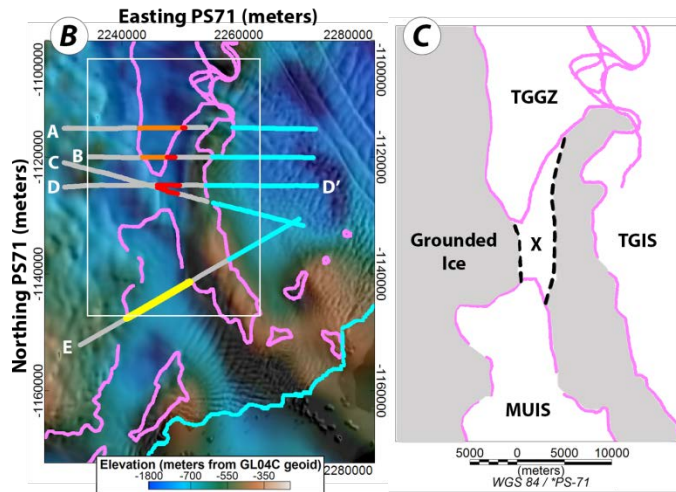


Figure 4 | Panels B and C from main text Figure 3 to show profile locations

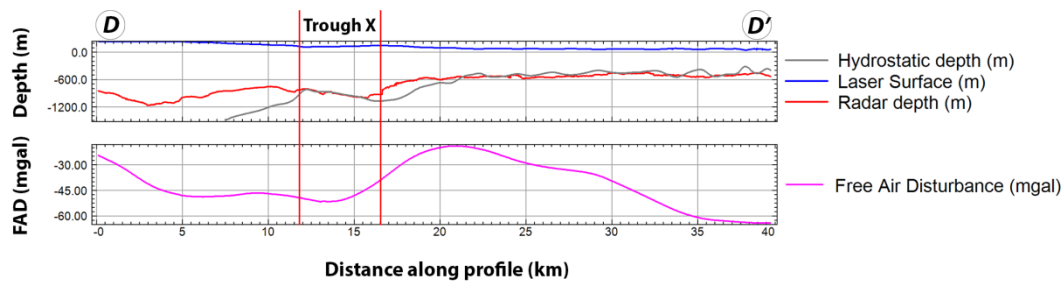


Figure 5 | Profile D-D': **Top plot**, Trough X lies where the ice bottom measured by radar sounding matches the depth predicted from the ice surface assuming floatation. **Bottom plot**, Free Air Disturbance indicates a short wavelength low for Trough X.

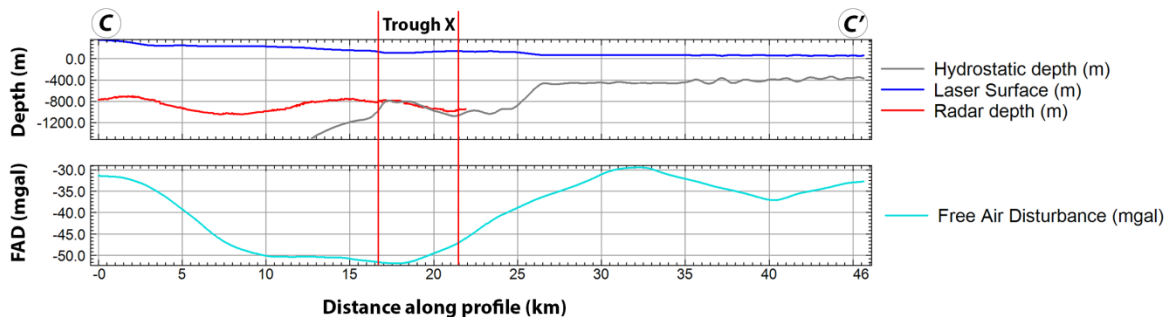


Figure 6 | Profile C-C': **Top plot**, Trough X lies where the ice bottom measured by radar sounding matches the depth predicted from the ice surface assuming floatation. **Bottom plot**, Free Air Disturbance indicates a short wavelength low for Trough X.

5. Grounded icebergs

Two video files have been included in the Supplementary Information composed of MODIS satellite radar imagery¹² compiled from 2002 to 2014 showing grounded icebergs near the calving fronts of the Totten Glacier and Moscow University ice shelves. The first frame of the Totten Glacier video begins with a map of the inverted bathymetry result with the MODIS Mosaic of Antarctica¹³ plotted as a transparent overlay. Each subsequent frame briefly shows each MODIS image stamped in the upper left corner with the MODIS filename of the image used for that frame which includes the date stamp. Each frame of the MUIS video includes the bathymetry result with each subsequent MODIS image plotted as a transparent overlay. The upper right corner of each frame includes the box names as indicated in Figure 7, below.

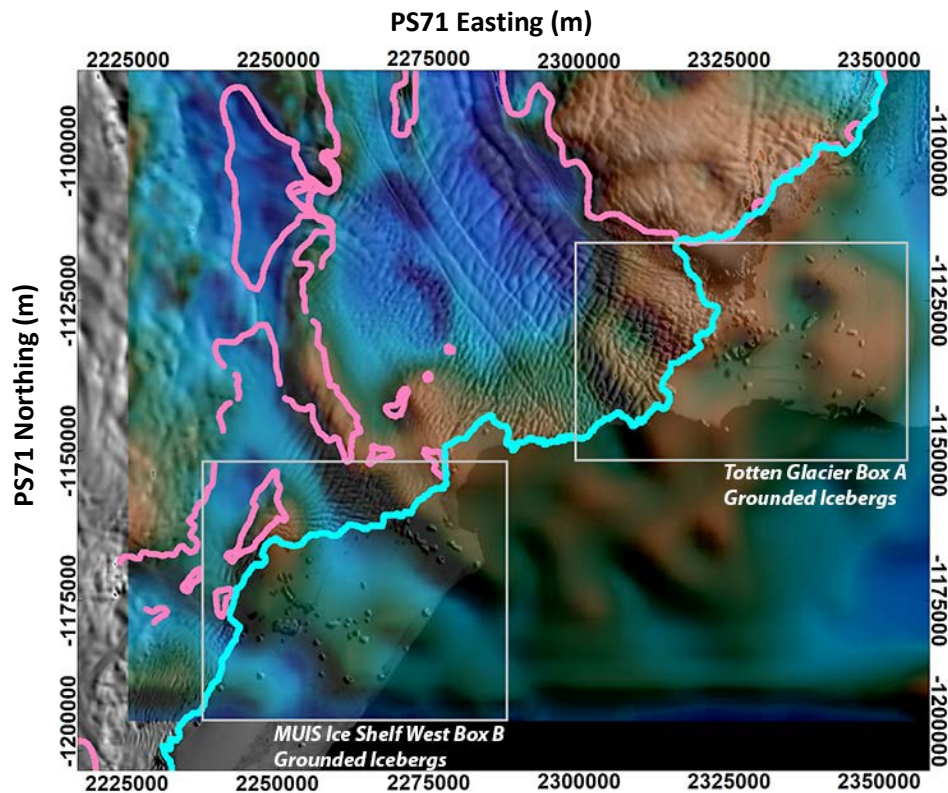


Figure 7 | Selection of the bathymetry inversion result with the MODIS MOA¹³ plotted as a partially transparent overlay. The two grey boxes indicate the areas where the Supplementary Videos show icebergs commonly grounded on shallow topography predicted by the bathymetry result.

6. Bed Reflection Coefficients:

Raw radar field data include reflection coefficients corrected for spreading loss between the transmitter and the bottom of the ice. To compute radar attenuation in the ice we first applied a firn correction to the raw ice thickness (which is reported without a firn correction) using a published conversion factor¹⁴ applied to the latest firn thickness compilation¹⁵. Ice attenuation was then computed using the mean, two-way reported value for ice shelves based on englacial attenuation modeling (30.2 ± 12.4 db/km)¹⁶.

7. Magnetics data and depth to magnetic basement solutions

Reliable depth to magnetic basement (DMB) solutions require a magnetics dataset that has been corrected for diurnal variations, inter-season variations in field intensity, and continuation effects from differences in acquisition height between flight lines. We used a subset of the corrected, leveled data and followed the same DMB approach presented in a recent study of the larger ICECAP survey area⁴. The DMB approach

applies 2D Werner deconvolution to compute solutions along each flight line in the survey area between 0.5 and 10km from the magnetics sensor. Each solution was corrected for flight elevation so that the results are shown with respect to the GL04C geoid. Errors in this technique will be between 20 and 40% of the source-sensor separation⁶ and were only used in this study to guide the geological model selection.

8. Sea Level Potential for Totten Glacier and the Aurora Subglacial Basin

We estimate the global sea level potential of ice flowing through Totten Glacier using a modified approach applied for Thwaites and Pine Island Glaciers^{17,18}. We find the ice volume¹⁹ within the Totten Glacier Catchment²⁰, correct for the higher density of seawater, subtract the volume of seawater required to replace the submarine ice, and divide the result by the area of the world oceans (3.6E14 m²). The result, ~3.5 meters, is conservative because it implies vertical catchment boundaries whereas, in reality, ice from neighboring catchments would contribute to the total sea level contribution if the entire catchment was drained of ice.

We follow a similar procedure to compute the total potential global sea level contribution of the Aurora Subglacial Basin (ASB) using catchment 13 defined on NASA Goddard Space Flight Center's drainage basin website²¹. Using that catchment we find that at least 5.1 m of global sea level potential is grounded below sea level and is therefore more susceptible to retreat. This figure assumes that all remaining ice grounded above sea level remains as it is today with unrealistic vertical cliffs. If all of the ice in the ASB were to melt, the total sea level contribution would be closer to 6.7 meters. The sea level figures here have not been corrected for isostatic rebound associated with the removal of ice loading of the crust.

9. Data Sources

All data used in this study are available for download from the National Snow and Ice Data Center:

<http://nsidc.org/>

References:

- 1 Cochran, J. R. & Bell, R. E. Inversion of IceBridge gravity data for continental shelf bathymetry beneath the Larsen Ice Shelf, Antarctica. *Journal of Glaciology* **58**, 540-552, doi:10.3189/2012JoG11J033 (2012).
- 2 Bourne, A. M. *et al.* Seabed topography beneath Larsen C Ice Shelf from seismic soundings. *The Cryosphere* **8**, 1-13, doi:10.5194/tc-8-1-2014 (2014).
- 3 Clark, D. J., Hensen, B. J. & Kinny, P. D. Geochronological constraints for a two-stage history of the Albany–Fraser Orogen, Western Australia. *Precambrian Research* **102**, 155-183, doi:[http://dx.doi.org/10.1016/S0301-9268\(00\)00063-2](http://dx.doi.org/10.1016/S0301-9268(00)00063-2) (2000).
- 4 Aitken, A. R. A. *et al.* The subglacial geology of Wilkes Land, East Antarctica. *Geophysical Research Letters* **41**, 2390-2400, doi:10.1002/2014gl059405 (2014).
- 5 Reading, A. M. The Seismic Structure of Wilkes Land/Terre Adelie, East Antarctica and Comparison with Australia: First Steps in Reconstructing the Deep Lithosphere of Gondwana. *Gondwana Research* **7**, 21-30, doi:10.1016/s1342-937x(05)70303-8 (2004).
- 6 Ku, C. & Sharp, J. Werner deconvolution for automated magnetic interpretation and its refinement using Marquardt's inverse modeling. *GEOPHYSICS* **48**, 754-774, doi:10.1190/1.1441505 (1983).
- 7 Rignot, E., Mouginot, J. & Scheuchl, B. Antarctic grounding line mapping from differential satellite radar interferometry. *Geophysical Research Letters* **38**, n/a-n/a, doi:10.1029/2011gl047109 (2011).
- 8 Bohlander, J. & Scambos, T. Antarctic coastlines and grounding line derived from MODIS Mosaic of Antarctica (MOA), Boulder, Colorado USA: National Snow and Ice Data Center. *Digital media* (2007).
- 9 Talwani, M., Worzel, J. L. & Landisman, M. Rapid gravity computations for two-dimensional bodies with application to the Mendocino submarine fracture zone. *Journal of Geophysical Research* **64**, 49-59, doi:10.1029/JZ064i001p00049 (1959).

- 10 Tsumuraya, Y., Tanahashi, M., Saki, T., Machihara, T. & Asakura, N. Preliminary report of the marine geophysical and geological surveys off Wilkes Land, Antarctica in 1983-1984. *Memoirs of National Institute of Polar Research. Special issue* **37**, 48-62 (1985).
- 11 Parker, R. L. The Rapid Calculation of Potential Anomalies. *Geophysical Journal of the Royal Astronomical Society* **31**, 447-455, doi:10.1111/j.1365-246X.1973.tb06513.x (1973).
- 12 Scambos, T., Bohlander, J. & Raup, B. Images of Antarctic Ice Shelves. 2002-2014 Boulder, Colorado, USA: National Snow and Ice Data Center. Digital media. http://nsidc.org/data/iceshelves_images/. (1996).
- 13 Scambos, T. A., Haran, T. M., Fahnestock, M. A., Painter, T. H. & Bohlander, J. MODIS-based Mosaic of Antarctica (MOA) data sets: Continent-wide surface morphology and snow grain size. *Remote Sensing of Environment* **111**, 242-257, doi:<http://dx.doi.org/10.1016/j.rse.2006.12.020> (2007).
- 14 Dowdeswell, J. A. & Evans, S. Investigations of the form and flow of ice sheets and glaciers using radio-echo sounding. *Reports on Progress in Physics* **67**, 1821 (2004).
- 15 van den Broeke, M. Depth and Density of the Antarctic Firn Layer. *Arctic, Antarctic, and Alpine Research* **40**, 432-438 (2008).
- 16 Matsuoka, K., MacGregor, J. A. & Pattyn, F. Predicting radar attenuation within the Antarctic ice sheet. *Earth and Planetary Science Letters* **359–360**, 173-183, doi:<http://dx.doi.org/10.1016/j.epsl.2012.10.018> (2012).
- 17 Holt, J. W. *et al.* New boundary conditions for the West Antarctic Ice Sheet: Subglacial topography of the Thwaites and Smith glacier catchments. *Geophysical Research Letters* **33** (2006).
- 18 Vaughan, D. G. *et al.* New boundary conditions for the West Antarctic ice sheet: Subglacial topography beneath Pine Island Glacier. *Geophysical Research Letters* **33** (2006).
- 19 Fretwell, P. *et al.* Bedmap2: improved ice bed, surface and thickness datasets for Antarctica. *The Cryosphere* **7**, 375-393, doi:10.5194/tc-7-375-2013 (2013).
- 20 Roberts, J. *et al.* Refined broad-scale sub-glacial morphology of Aurora Subglacial Basin, East Antarctica derived by an ice-dynamics-based interpolation scheme. *The Cryosphere* **5**, 551-560 (2011).
- 21 Zwally, H. J., Giovinetto, M. B., Beckley, M. A. & Saba, J. L. Antarctic and Greenland Drainage Systems, GSFC Cryospheric Sciences Laboratory, at http://icesat4.gsfc.nasa.gov/cryo_data/ant_grn_drainage_systems.php. (2012).